FORMATION OF COMPACT AND GAIABH-LIKE BINARIES IN YOUNG OPEN STAR CLUSTERS: EARLY EVOLUTION

by

Yersultan Tleukhanov

A Thesis Submitted to the Faculty of the

DEPARTMENT OF PHYSICS

In Partial Fulfillment of the Requirements
For the Degree of

MASTER OF SCIENCE

In the School of Science and Humanities

NAZARBAYEV UNIVERSITY

2026

NAZARBAYEV UNIVERSITY, SCHOOL OF SCIENCE AND HUMANITIES

As members of the thesis committee, we certify that we have read the thesis prepared by Yersultan Tleukhanov entitled

FORMATION OF COMPACT AND GAIABH-LIKE BINARIES IN YOUNG OPEN STAR CLUSTERS: EARLY EVOLUTION

and recommend that it be accepted as fulfilling the thesis requirement for the degree of Master of Science.

_____ Date: May 5, 2026

_____ Date: May 5, 2026

_____ Date: May 5, 2026

Final approval and acceptance of this thesis is contingent upon the candidate's submission of the final copies of the thesis to the Department of Physics.

I hereby certify that I have read this thesis prepared under my direction and recommend that it be accepted as fulfilling the thesis requirement.

_____ Date: May 5, 2026
Thesis Director: Bekdaulet Shukirgaliyev

TABLE OF CONTENTS

ABSTRACT

Gaia's third data release found three wide, dormant black hole binaries: GaiaBH1, GaiaBH2, and GaiaBH3. isolated binary evolution models don't reproduce similar orbital properties. Most simulated Milky Ways yield nearly zero detectable systems like these. Dynamical formation in young star clusters does better, producing Gaia-like binaries up to a thousand times more efficiently per unit of stellar mass. This thesis explores what this formation channel will yield in a realistic environment, using N-body simulations of open clusters that undergo instantaneous gas expulsion. We ran 81 star cluster simulations. The pipeline combines MCLUSTER for initial mass and binary distributions, the AGAMA library for phase-space sampling in a residual gas potential, and PeTar with SSE/BSE stellar evolution. Every cluster has a star formation efficiency of $SFE = 0.17$, a primordial binary fraction of $f_b = 0.5$, and solar metallicity ($Z = 0.02$). They sit in a Milky Way-like tidal field at roughly 8 kpc from the Galactic center. Initial mass and phase-space random seeds are the only things that vary between runs. Each cluster evolved for 150 Myr, with snapshots saved every 1 Myr. We tracked black hole–star, neutron star-star, and black hole–black hole binaries, classifying each as primordial, dynamical, retained, or escaped. Across the 81 runs, the simulations produced 4006 binary systems, mostly primordial, including 271 black hole–star and 144 black hole–black hole pairs. Black hole–luminous companion binaries tend toward orbital periods of $170 - 200$ days, near-zero eccentricities, and companion masses of $1.0 - 1.2\ M_\odot$. These are within Gaia's detectability window but still don't match the observed systems well enough. The bottleneck is the mass-ratio distribution ($q \in [0.1, 1]$), which doesn't generate the extreme mass-ratio progenitors ($q \sim 0.03 - 0.05$) that Gaia-like systems require. Getting there means trying different pairing prescriptions, exploring lower metallicities, and running bigger simulations.

1 INTRODUCTION

1.1 X-ray Surveys

Historically, the majority of black holes have been discovered through X-ray surveys of the sky, which detect X-ray emission from mass accretion onto compact objects in binary systems [1]. Different survey techniques have revealed different pieces of the black hole population. The first solid evidence for supermassive black holes (SMBHs) came from watching stars orbit the Galactic Centre [2] and from recognizing that active galactic nuclei (AGNs) and quasars are black holes actively accreting [3]. The Sloan Digital Sky Survey (SDSS) [4] produced the first complete quasar samples at $z \gtrsim 6$, showing billion-solar-mass black holes existed within the first Gyr of the universe. Optically selected samples miss obscured AGN [5], so hard X-ray surveys were essential. The Chandra Deep Fields pushed to flux limits of $\sim 6 \times 10^{-17}\,\mathrm{erg\,cm^{-2}\,s^{-1}}$ [6], finding AGN at $z > 4$ and revealing X-ray-bright galaxies invisible in optical data. These surveys gave us a workable picture of cosmic black hole growth. But black holes not actively accreting remained an observational challenge.

1.2 Gravitational Wave Astrometry

A new window opened with gravitational wave detections from merging stellar-mass black holes. The first event, GW150914, recorded by LIGO [7], provided unambiguous evidence for stellar-origin black holes exceeding $\sim 20\,M_\odot$ and subsequent LIGO-Virgo-KAGRA observations revealed a mass distribution extending to $\sim 90\,M_\odot$ [8]. These detections raised the question of which stellar populations produce such massive remnants. Gravitational wave observations are, however, sensitive only to compact binaries in the final stages of inspiral. They provide no information on wider-orbit progenitor systems

However, the third data release of the Gaia Mission has revealed a new method for discovering black holes through precise binary orbital measurements [9]. As of the latest data release, three strong candidates for black hole binaries identified through Gaia astrometry have been reported [9–11]. The third Gaia data release yielded the first two dormant black holes in the Milky Way: Gaia BH1 [9] and Gaia BH2 [10]. These systems present in the solar neighborhood yet undetected throughout decades of X-ray monitoring. Pre-release DR4 astrometry subsequently revealed Gaia BH3, a $33\,M_\odot$ black hole orbiting a metal-poor giant with $[\mathrm{M/H}] \approx -2.5$ at $\sim 2\,\mathrm{kpc}$ [11]. The images of their luminous companions are presented in Figure 1, and thier orbital parameters are presented in Table 1

Table 1: Main properties of Gaia BH1 [9], Gaia BH2 [10], and Gaia BH3 [11].

	Stellar Type	M_{BH} ($M_\odot$)	M_* ($M_\odot$)	a ($R_\odot$)	P (days)	e	[Fe/H]
Gaia BH1	G-type main sequence	$9.62^{+0.18}_{-0.18}$	$0.93^{+0.05}_{-0.05}$	$301.55^{+2.15}_{-2.15}$	$185.59^{+0.05}_{-0.05}$	$0.45^{+0.005}_{-0.005}$	-0.2
Gaia BH2	Red giant	$8.94^{+0.34}_{-0.34}$	$1.07^{+0.19}_{-0.19}$	$1066.55^{+17.20}_{-17.20}$	$1276.7^{+0.6}_{-0.6}$	$0.5176^{+0.0009}_{-0.0009}$	-0.2
Gaia BH3	G-type giant	$32.7^{+0.82}_{-0.82}$	$0.76^{+0.05}_{-0.05}$	$2477.0.35^{+58.058}_{-58.058}$	$4253.1^{+98.5}_{-98.5}$	$0.7291^{+0.0048}_{-0.0048}$	-2.6

1.3 Formation of Gaia-type Black Holes

Despite these detections, current formation models of binary systems struggle to reliably predict the detection of black hole-star systems with Gaia-like parameters [12]. These Gaia detections have motivated significant theoretical interest in understanding how such wide binary systems form. Furthermore, Rastello et al. [13] demonstrated in their simulations of star clusters that binaries with parameters similar to Gaia BH1 only become detectable after a post-common-envelope system undergoes gravitational exchanges with other stars in a cluster environment. Additionally, some simulations formed Gaia-like binaries only in low metallicity clusters, which contrasts with the high metallicity measured for Gaia BH1 and Gaia BH2 [14].

Moe & Di Stefano [15] compiled early-type binary populations and found that companion frequency scales with primary mass. Solar-type primaries have a companion frequency around 0.50, while O-type stars reach 2.1. This means most black hole progenitors evolve with close stellar companions, not in isolation.

There are three distinct formation channels recognized in the literature: Isolated Binary Evolition, Hierarchical triple-star evolution, Dynamical formation in star clusters.

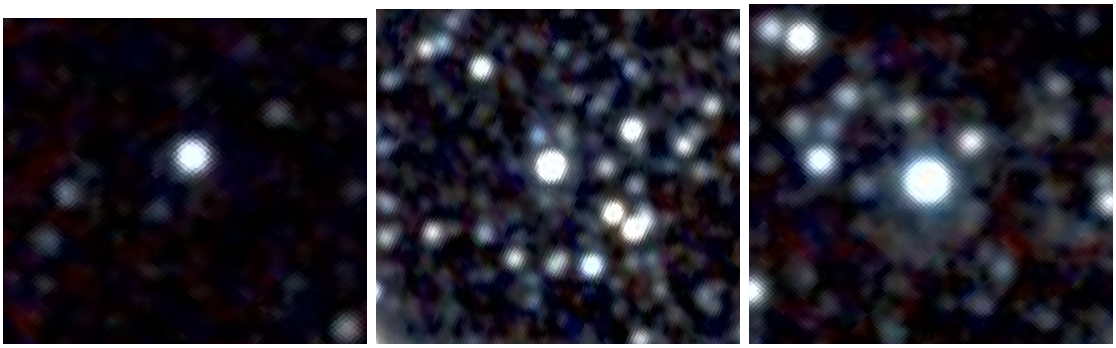

(a) GaiaBH1 (b) GaiaBH2 (c) GaiaBH3

Figure 1: These are images of luminous companions of GaiaBH1, GaiaBH2, GaiaBH3 made by Two Micron All-Sky Survey (2MASS) and taken from Aladin an interactive sky atlas

Isolated binary evolution

The isolated binary evolution (IBE) channel has been the go-to model for BH–stellar binary formation for years. But it can't explain what Gaia found. Gaia BH1 and Gaia BH2 each host a $\approx 9\ M_\odot$ black hole on a wide, eccentric orbit around a low-mass companion—186 days and 1277 days respectively. These fall squarely in the 10^2–10^4 day period range where IBE models predict almost nothing [12]. The issue lies in the common envelope phase. When the massive BH progenitor overflows its Roche lobe onto a $\approx 1\ M_\odot$ companion, the inspiral should shrink the orbit by a factor of $100 - 1000$. Post-CE separations should end up at least 50 times smaller than what we observe [10]. Even tweaking CE efficiency or adding pre-CE wind mass loss cutting the envelope to just $\approx 3\ M_\odot$ the numbers still don't work. And there's no well-motivated physical mechanism for $\alpha_{CE} > 1$ [16]. The rates are equally grim. Nagarajan et al. [12] ran the Gaia DR3 selection function against Chawla et al.'s IBE population. In most simulated Milky Ways, the model predicts zero detectable BH binaries. Eight out of 100 trials produced one—but only for companions far more luminous than anything Gaia BH1 or BH2 show.

Kotko et al. [16] calculated intrinsic formation rates: $\approx 3.2 \times 10^{-10}\ M_\odot^{-1}$ for Gaia BH1-like systems, $\approx 1.4 \times 10^{-10}\ M_\odot^{-1}$ for Gaia BH2-like. That's at most ≈ 900 detectable systems across the entire Galactic thin disc. Gaia BH2 is the harder case—it needs the natal kick within 15^o of the orbital plane at roughly 20 $\frac{km}{s}$. As Nagarajan et al. [12] note, IBE predictions for Gaia-detectable BHs "have generally become more pessimistic over time."

Hierarchical triple-star evolution

Few-body gravitational interactions have been shown to play a crucial role in the formation of star systems with unusual parameters [17]. For many massive stars, long-period companions at $\log P \approx 5.5$–7.5 ($a \approx 200$–5000 au) are outer tertiary components in hierarchical triples. About 55% of O-star primaries have two or more companions [18]. Li et al. found one working configuration: a triple with masses 9.03 $M_\odot$, 3.12 $M_\odot$, and 1.00 $M_\odot$, inner and outer periods of 2.21 and 121.92 days [19]. TEDI-driven merger plus CHE of the 12.11 $M_\odot$ product ($\Omega_{crit} = 0.8$, $B_o = 5000\ G$) yields a post-merger binary matching Gaia BH1's orbit—if the supernova or failed supernova kicks out only $\approx 0.22\ M_\odot$. The rates are where things fall apart. Generozov & Perets evolved $\approx 10^6$ triples and got at most $\approx 2.9 \times 10^{-7}\ M_\odot^{-1}$ for Gaia BH1-like systems [20]. As Generozov & Perets note, more simulations are needed [18]. Small-number statistics and poorly understood merger product evolution keep the model constrained.

Li et al. have the same issue. Post-merger stars need rapid rotation ($\Omega_{crit} \approx 0.8$) and strong magnetic fields ($B_o \approx 5000$ G) [19]. They've tested one set of initial conditions.

Dynamical formation in star clusters

Rastello et al. found young star clusters form Gaia BH1-like systems about two orders of magnitude more efficiently per unit stellar mass than isolated binary evolution: roughly $2 \times 10_{-7}\ M^{-1}$ for ejected systems [13]. Di Carlo et al. scaled to a full Milky Way and found the dynamical channel is roughly 50 times more efficient overall [21]. Even with only 10% of star formation in young clusters, about four out of five BH-stellar binaries in the Galaxy form dynamically — roughly 2×10^5 total. Tanikawa et al. was able to obtain open cluster rates around $10^{-5}\ M^{-1}$, exceeding isolated binary evolution by three orders of magnitude [22].

Dynamical channels also uniquely occupy the period-eccentricity space where Gaia BH1 and Gaia BH2 actually sit. Di Carlo et al. showed that any detectable BH binary older than 100 Myr with $e > 0.5$ or $M_{BH} > 10\ M_\odot$ must be dynamically formed [21]. Nagarajan et al. applied Gaia's selection function and found the dynamical model produces a roughly log-uniform period distribution, right where Gaia is sensitive, while isolated binary evolution predicts a gap, yielding zero detections in 92 out of 100 simulated Milky Ways [12]. Fantocobi et al. ran N-body simulations of massive star clusters ($M_c = 10^4 - 10^6\ M_\odot$) and obtained two Gaia BH1-like systems, both dynamically formed. Gaia BH2-like systems also appeared, with efficiency $\approx 4.4 \times 10^{-7}\ M_{-1}$ [14]. Nagarajan et al. found the Di Carlo et al. model overpredicts DR3 orbital solutions by a factor of ≈ 8 [12, 21]. Normalization still needs work [12, 21]. Fantocolli et al. note their candidates form in low-metallicity clusters ($Z = 0.001$), slightly at odds with the observed near-solar metallicities ($[Fe/H] \approx -0.2$) [14]. These findings support further investigation of star cluster models for formation of Gaia-like binaries.

1.4 Aims of the work

The aim of this thesis is to explore a possible formation track for Gaia-like black holes through modern N-body simulation methods where a star cluster undergoes a gas expulsion and is placed in a galactic potential. We use MCLUSTER to generate mass distributions, binary pair distribution, and distribution of binary orbital parameters such as eccentricity, mass ratio, semi-major axis. Phase-space for the particles is generated AGAMA module, where the gas expulsion aspect is emulated through velocity is distributed in a residual gas + stars potential. All of that information is passed to PeTar, a highly accurate N-body solver. It accurately simulates the short and long range interactions, employs stellar evolution models, and allows to place a star cluster in a Milky Way-like potential. Moreover, PeTar provides a wide array of tools for tracking individual stars and their properties. We simulate 81 clusters with the same properties except for mass and phase-space randomizations. We gather the data on binary populations of

these clusters and asses the orbital parameter distributions over time. We compare their parameters to parameters of GaiaBH1 and GaiaBH2. In addition, we explore formation of compact binaries that may produce a mereger event.

Table 2: Common initial conditions passed to MCLUSTER

Option	Set Value	Explanation
n_i	20000	Initial number of objects for each sub-population
f_b	0.5	Primoridal binary fraction
InitialModel	1	Initial density distribution. Plummer model was chosen.
S	0.0	Mass segregation parameter. Chosen value means no segregation
fractal	C	Fractal dimensions. Chosen option means no fractal dimensions
q_{vir}	0.5	Virial ratio is set to 0.5 so the system is in virial equilbrium
m_{func}	1	Stellar mass function for initial mass distribution. Kroupa IMF was chosen
pairing	3	Pairing of binary components. Chosen option follows works of Kiminki & Kobulnicky [26]; Sana et al., [27]; Kobulnicky et al., [28]. Meaning, uniform distribution of mass ratio (0.1 ¡ q ¡ 1.0) for $M > 5\ M_\odot$ and random pairing for remaining particles
adis	6	Semi-major axis distribution. Chosen option is the following distribution: uniform distribution in log(a), between amin and amax for $M < 5\ M_\odot$; Sana et al. [27] period distribution for $M > 5\ M_\odot$
eigen	Off	Eigenevolution is off, as I want unevolved stars at the begining of a simulation
a_min	1 AU	Minimum binary semi-major axis. Set values is given to MCLUSTER in solar radii, $R_\odot$.
a_max	1000 AU	Maximum binary semi-major axis. Set values is given to MCLUSTER in solar radii, $R_\odot$.
t_f	1	point mass galaxy
rh_mcl	1.0	Hlaf mass radius in pc
epoch	0	Age of population in Myr
Z	0.02	Initial metallicity
seedmc	9 random seeds	Initial integer number to start random number generator for Mcluster initial conditions. Nine integer numbers were used to initialize random number generator.

2 METHODS

This section describes the methods used to prepare and simulate the evolution of our star cluster model. Initial conditions are only varied in initial phase space and initial mass distribution. The generated initial conditions then are passed down to PeTar to evolve in a GPU-accelerated N-body simulation. All of the output data is then analyzed through python scripts with PeTar's own python module, which aimed to assist the work with output data.

2.1 Initial Conditions

Initial conditions are prepared using Python algorithm combining MCLUSTER [23] with the `agama` galactic dynamics library [24]. This produces a self-consistent equilibrium model accounting for stellar mass distribution and residual gas potential.

Initial parameter space - mass (m), metallicity (Z), semi-major axis (a), mass ratio (q) - is handeled through MCLUSTER. Common initial parameters are listed in Table 2. Stellar masses drawn from the Kroupa [25] initial mass function with limits $0.08\ M_\odot \leq M \leq 150\ M_\odot$.

For each pair of phase space and mass randomizations, the same parameters were used. After the MCLUSTER generates a cluster population, the binary population is filtered by primary mass to track dynamical black hole binary formation. A mass threshold $M_{thresh} = 10.0\ M_\odot$ applies to primordial pairs. Binaries with primary above this

threshold stay bound; below it, the binary breaks into isolated single stars. Each cluster undergoes instantaneous gas expulsion following the model of Shukirgaliyev et al. [29], where the residual gas mass is removed at the start of dynamical evolution. The clusters are embedded in a galactic tidal field at a Galactocentric distance similar to that of the solar system ($R_G \approx 8$ kpc).

The total density profile is the sum of the density profiles of the residual gas, ρ_{gas}, and the embedded cluster, ρ_*, at any time:

$$\rho_0(r) = \rho_{gas}(t, r) + \rho_*(t, r); \tag{1}$$

here r if the distance from the clump center. The density of the pure gas at time t is given by Eq.(19) from Parmentier and Pflanzer:

$$\rho_{gas}(t, r) = \left(\rho_0(r)^{-\frac{1}{2}} + \sqrt{\frac{8G}{3\pi}}\epsilon_{ff} t\right)^{-2}. \tag{2}$$

G is the gravitational constant and ϵ_{ff} is the SFE per free-fall time.

The aim of these models is to investigate the stellar evolution of such binary systems after instantaneous gas expulsion. Thus, our approach is to adopt a well documented star density profile and derive initial gas density through it and Eq. 2. For our star density profile, we took Plummer [30] model:

$$\rho_*(r) = \frac{3M_*}{4\pi a_*^3}\left(1 + \frac{r^2}{a_*^2}\right)^{-\frac{5}{2}}. \tag{3}$$

M_* is the total mass of the star cluster and a_* is the Plummer radius. The latter a_* is directly proportional to the half-mass radius of the cluster. I chose the Plummer model because it has an analytical expression, and we may consider a certain finite mass for gas and stars. Moreover, the model is supported by a wide range of N-body simulation codes, which makes it possible to accurately compare our results to results from different works. Now what is left is to take the star density profile, $\rho_*(r)$,

$$\rho_0(r, t_{SF}) = \rho_{gas}(r, t_{SF}) + \rho_*(r); \tag{4}$$

$$\rho_{gas}(r, t_{SF}) = \left((\rho_{gas}(r, t_{SF}) + \rho_*(r))^{-\frac{1}{2}} + \sqrt{\frac{8G}{3\pi}}\epsilon_{ff} t_{SF}\right)^{-2}. \tag{5}$$

In this equation, t_{SF}, the star formation duration is given in units of Myr if densities of stars, ρ_*, and residual gas ρ_{gas} are measured in $M_\odot\ pc^{-3}$, and the gravitational constant is $G = 0.0045\ pc^3\ M_{sun}^{-1}\ Myr^{-2}$. Eq. 5 has an analytical solution for stellar density, which was taken from Shukirgaliyev, B. [31]:

$$\rho_{gas} = \frac{1}{k^2} - \frac{\rho_*}{2} - \frac{1}{2}\sqrt{K_2 + \frac{8}{k^6 K_1}} + K_1. \tag{6}$$

Here, $k = \sqrt{\frac{8G}{3\pi}}\epsilon_{ff} t_{SF}$, and $K_{1,2}$ are terms dependent on k and ρ_*. For the sake of clarity, we show Eq. 13-16:

$$\alpha = k^4 \rho_*^2; \tag{7}$$

$$K_0 = \sqrt[3]{\alpha^3 + 36\alpha^2 + 216\alpha + 24\alpha\sqrt{3(\alpha + 27)}}; \tag{8}$$

$$K_1 = \sqrt{\frac{\alpha^2 + \alpha(K_0 + 24) + K_0(K_0 + 12)}{12k^4 K_0}}; \tag{9}$$

$$K_2 = \frac{(\alpha - K_0 + 24)(k_0 - \alpha)}{3k^2 K_0} \tag{10}$$

This certain solution decreases as we move away from the center of the star forming region, which follows the behavior of centrally concentrated star forming regions where stellar density decreases with increasing radius. This analytic density profile of a residual gas is then passed to `AGAMA` to generate an effective potential.

The initial positions and velocities of stellar particles are generated using the `AGAMA` stellar dynamics library, following a self-consistent phase-space sampling procedure. The gravitational potential of the gas component is constructed numerically via a spherically symmetric multipole expansion of the gas density profile ρ_{gas} from Eq. 6, evaluated over a prescribed radial grid from r_{min} to r_{max}, while the stellar potential is represented analytically by a Plummer sphere of total mass M_s and Plummer radius a. These two components are superposed to form the total gravitational potential Φ_{total}, which captures the combined dynamical influence of both the stellar and gaseous mass distributions. A quasi-spherical distribution function $f(E, L)$ for the stellar population is then constructed, self-consistently reproducing the Plummer stellar density profile within Φ_{total}, thus ensuring that the stars are initialised in dynamical equilibrium with the full two-component potential rather than their self-gravity alone. This distribution function and the total potential are encapsulated in an AGAMA GalaxyModel object, from which N phase-space particles, described by a position and velocity vector (x, y, z, v_x, v_y, v_z), are sampled, yielding a set of initial phase space. Then, these positions and velocities are then replace the ones generated by MCLUSTER. For binary particles, the center of mass positions and velocities are replaced.

Data formats for PeTar ingestion. If an external galactic tidal field applies (Galactocentric radius X_{sc}, velocity V_{sc}), the cluster's half-mass radius r_h scales to fraction λ of theoretical Jacobi tidal radius r_J. Output writes to petar.init-compatible 7-column format for simulation launch.

McLuster produces raw structural and kinematic data, but PeTar needs specific data structures. The `petar.init` preprocessing tool handles this translation. McLuster outputs phase-space coordinates for each star: mass, three-dimensional position and velocity. For primordial binaries, binary components appear on adjacent lines at the file's start.

The `petar.init` reads the first $2 \times N_b$ rows to initialize hierarchical binary system structures before reading single stars. It also handles unit conversion. McLuster outputs in standard astronomical units ($M_\odot$, pc, $\frac{km}{s}$), but PeTar uses velocity in $\frac{pc}{Myr}$. The `-v kms2pcmyr` flag automatically converts all velocities. Mass and spatial coordinates stay in $M_\odot$ and parsecs for compatibility with embedded stellar evolution routines. This study tracks compact-object binary formation over cosmic time, so we enable PeTar's BSE implementation from $t = 0$. The `-s bse` flag appends necessary columns: Zero Age Main Sequence (ZAMS) mass, stellar type, fractional age, and internal structure. These let PeTar hand off particles to BSE routines during simulation run-time.

The cluster embeds in a realistic galactic environment using the Galpy potential library [32]. Since initialization happens in the center-of-mass frame, the -c and -t flags apply global position and velocity offsets to all particles. This places the cluster at the correct Galactocentric radius and assigns appropriate orbital velocity relative to the Galpy potential, letting PeTar compute tidal stripping and dynamical friction. Galpy uses simplified Milky Way-like potential fits described by Bovy et. al. [33].

2.2 PeTar Simulations

For the simulations in this work, we use PeTar [34], a high-performance N-body code for modeling massive collisional stellar systems like globular clusters. Star cluster simulations span vastly different timescales: binary orbital periods as short as a few days, stellar crossing times on the order of Myr, and two-body relaxation times of several Gyr. PeTar handles this by combining three methods within a Hamiltonian-splitting framework: the Barnes-Hut particle-tree (PT) for long-range interactions at O(N log N) cost, the fourth-order Hermite integrator with block time steps for short-range neighbor interactions, and the Slow-Down Algorithmic Regularization (SDAR) method for accurately integrating few-body systems and tight binaries. Compared to `nbody6++gpu`, PeTar handles an arbitrary fraction of primordial binaries and hierarchical multiple systems, and uses a mass-dependent changeover function that correctly treats wide mass spectra containing objects as massive as supermassive black holes. Benchmark tests show PeTar achieves up to ~ 11 times better performance than `nbody6++gpu` for million-body simulations with large binary fractions, and scales to 10^7 particles on modern supercomputers using hybrid MPI, OpenMP, SIMD (AVX/AVX-512), and GPU (CUDA) parallelization.

Stellar Evolution

For the purposes of understanding the evolution of stellar systems, it is necessary to adhere to stellar evolution models that will enrich interactions of stars beyond point mass simulations. For our simulations we have chosen a SSE/BSE model developed by Banerjee

et. al. [35].

Banerjee's updated SSE/BSE implementation produces realistic masses and velocities for compact remnants (black holes, neutron stars) across a wide range of initial stellar masses and metallicities [35]. For stellar winds that set up the pre-supernova structure, the code uses the semi-empirical prescriptions from Belczynski et al. [36] for massive stars and their evolved phases, replacing the older wind treatment of Hurley et al. [37]. On the remnant side, it drops the simple old prescriptions in favor of the core-collapse models of Fryer et al. [38], so the final compact-object mass depends on the full prior stellar evolution rather than a simple mapping from initial mass.

Core-collapse events use the "rapid" and "delayed" explosion models of Fryer et al. [38], combined with treatments of pulsational pair-instability and full pair-instability supernovae following Belczynski et al. [39]. For each collapsing star, the code computes a proto-remnant mass and fallback fraction as functions of the carbon-oxygen core mass and pre-supernova mass, then applies the Belczynski et al. [39] criteria to decide when pulsational pair-instability reduces the final black hole mass or when full pair-instability removes the star entirely. This reproduces modern initial-final mass relations, including a maximum black hole mass and a pair-instability gap.

Beyond the mass prescription, Banerjee et al. [35] implement natal kick models tied to fallback and different physical mechanisms. A fallback-modulated, momentum-conserving kick prescription serves as the baseline. They also include recipe-based versions of convection-asymmetry-driven, collapse-asymmetry-driven, and neutrino-driven kicks from the core-collapse literature. Applied to cluster models, the resulting retention fractions and mass distributions differ strongly between kick models — collapse-asymmetry kicks retain nearly all black holes, while neutrino-driven kicks eject almost all.

2.3 Data Analysis

Each run has ran for 150 Myr, and data files were written out every Myr. Hence, every run had 150 snapshot files. Since the BSE and Galpy external potential were enabled, the data files contain additional columns covering the stellar evolution of each particle (binary/single), and it contains columns tracking the external potential relative to the particles. Once the run is finished, I employed PeTar's helper script `petar.gether` that gather information on binary population, single population at each snapshot. Then, I use PeTar's `petar.process` script to generate data files on binary/single type change events, escaped binary systems, cluster core information.

All of this data is then fed through a series of my python scripts in an interactive python notebook. I tracked binary systems by their ids and assigned the following categories: primordial, escaped, BH-Luminous, NS-Luminous, BH-BH. Primordial binaries are binary systems which id pairs were present in the initial snapshot. Escaped binaries are flagged

if they have an escape time and their escape time is less than the snapshot time. BH-Luminous and NS-Luminous statuses are assigned when at least on of the stars is of corresponding type (BH - black hole, NS - neutron star), and then when at least one of the stars has a luminance higher than 0.1 $L_\odot$. The BH-BH status is assigned when both of the components has type BH.

For the purposes of assessing possible compact object mergers, I have used time to coalescence, T_{merge},approximations for eccentricities close to zero from P. C. Peter:

$$T_{merge}(e_0) = T_{circ}(a_0) \times f(e_0) \tag{11}$$

$$T_{circ}(a_0) = \frac{12}{19} \cdot \frac{a_0^4}{4\beta} \tag{12}$$

$$\beta = \frac{64}{5} \frac{G^3 m_1 m_2 (m_1 + m_2)}{c^5} \tag{13}$$

$$f(e) \approx \frac{(1-e^2)^{\frac{7}{2}}}{1 + \frac{73}{24}e^2 + \frac{37}{96}e^4}. \tag{14}$$

$T_{circ}(a_0)$ is a special case for circular orbits. $f(e)$ is an approximation factor that helps computing approximate values of T_{merge} around small eccentricities ($e \sim 0.2 - 0.3$). This value is computed for all entries.

3 RESULTS

This section covers the results from the 81 star cluster simulations evolved till 150 Myrs. Overall, our simulations have produced 4006 binary systems, both hard and wide. Table 3 holds count of total number, minimum and maximum count per cluster, and mean/median per cluster of all binaries and several sub-populations from our simulations. For each binary type: black hole-star (BH-S), neutron star-star (NS-S), and black hole-black hole (BH-BH), the table lists the total number of systems, the range of systems per cluster, and the mean/median number per cluster. Binaries are separated into primordial and dynamical populations. Moreover, I have looked at distributions of five parameters, namely: Initially primary mass (m_1), Eccentricity (e), Semi-major axis (a), Orbital period (P), Initially companion mass (m_2). These five parameters are assessed for seven populations of binary systems at three snapshots ($T = [50, 100, 150]\ Myr$) across all realizations.

3.1 Binary Parameters Distribution

Figure 3 shows primary mass m_1, eccentricity e, semi-major axis $\log[a]$, orbital period $\log[T_{\rm orbital}]$, and secondary mass m_2 for all BH binaries across 81 realisations, at 50, 100, and 150 Myr. Primary mass splits into two peaks: low masses ($m_1 \lesssim 2\,M_\odot$) dominate, and there's a secondary group at 7–10 $M_\odot$. Eccentricity bunches toward low values ($e \lesssim 0.2$)

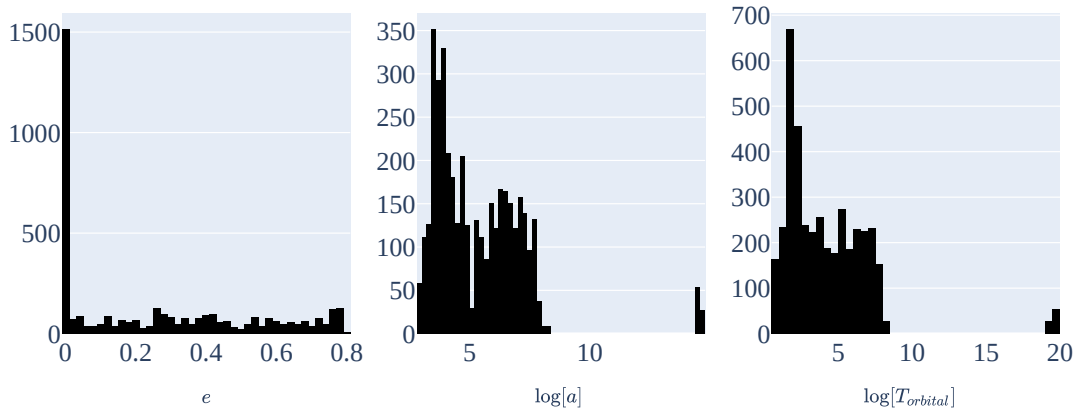

Figure 2: These are distributions of eccentricity (e, left panel), semi-major axis (a, middle panel), and orbital period (T, right panel) at the initial snapshot. The semi-major axis and the orbital period are scaled logarithmically.

Table 3: Population statistics of compact binaries across simulated star clusters.

		Total number	Range per cluster	Mean/Median
All Binary Systems		4006	39-66	49.46/48.00
	BH-S	271	1-5	3.35/3.00
	NS-S	484	2-10	5.97/5.00
	BH-BH	144	1-3	1.78/2.00
Primordial Binaries		3843	37-64	47.5/46
	BH-S	261	1-5	3.2/3.00
	NS-S	484	2-10	5.97/5.00
	BH-BH	135	0-3	1.67/2.00
Dynamical Binaries		163	0-5	2.01/2.0
	BH-S	10	0-1	0.12/0.00
	NS-S	0	0	0.00/0.00
	BH-BH	9	0-1	0.11/0.00

at all epochs, but there's a tail of high-eccentricity systems ($e \gtrsim 0.6$). Semi-major axis and orbital period are bimodal as well. Compact group: $\log[a] \sim 0$–2 ($a \sim 1$–$100\,R_\odot$, $\log[T_{\rm orbital}] \sim -2$–$2$ days). Wide group: $\log[a] \sim 5$–6 ($\log[T_{\rm orbital}] \sim 8$–$10$ days). Count grows from 50 to 150 Myr. Most of the growth is in the low-m_1 and wide-orbit populations.

Primordial and Dynamical

Figure 4 shows primordial black hole binaries at 50, 100, and 150 Myr. Primary mass is broad, 0–10 $M_\odot$, with a low-mass peak at $m_1 \lesssim 2\,M_\odot$ and a high-mass one at $m_1 \sim 7$–$9\,M_\odot$. Primordial binaries make up most of the binary population. Eccentricities distirbuted near zero. Semi-major axes split into two groups: compact at $\log[a] \sim 0$–2, wide at $\log[a] \sim 5$–6. Secondary mass m_2 is bimodal—$m_2 \lesssim 1\,M_\odot$ and

$m_2 \sim 6$–$8\,M_\odot$—low-mass stars to compact objects.Count grows from 50 to 150 Myr. New BH systems keep coming from the primordial binary pool as the cluster evolves. Now for the dynamically formed binaries (Fig 5), the population size is smaller than primordial population (peak $\lesssim 80$ vs. ~ 400–500 primordial), and primaries are massive, $m_1 \sim 6$–$10\,M_\odot$. Eccentricity is broad and nearly uniform, $e \sim 0$–0.9. Semi-major axes at intermediate-to-wide ($\log[a] \sim 1$–2), orbital periods at $\log[T_{\rm orbital}] \sim 0$–$1$ days. Dynamical formation does not make very tight binaries in the first 150 Myr. Secondary mass m_2 also high, $m_2 \sim 5$–$8\,M_\odot$.

Retained and Escaped

Figure 6 shows black hole binaries that remain gravitationally bound to the cluster, at 50, 100, and 150 Myr. Retained primaries sit at high masses ($m_1 \sim 7$–$9\,M_\odot$). The 50 Myr is the only snapshot with substantial numbers. The retained binary counts drop at 100 and at 150 Myr. Possibly, they get disrupted by dynamical encounters or escape into galactic potential. Eccentricity spans $e \sim 0$–1. Semi-major axes cluster at intermediate separations ($\log[a] \sim 1$–2, $a \sim 10$–$100\,R_\odot$). Secondary masses are $m_2 \sim 6$–$8\,M_\odot$, so BH–BH or BH–massive-star pairs dominate. Orbital periods peak at $\log[T_{\rm orbital}] \sim 0$–$1$ days. Now for the escaped population (Fig. 7), the escaped count is way higher than retained (peak ~ 400 at 150 Myr), and it's dominated by low-mass primaries ($m_1 \lesssim 2\,M_\odot$). Eccentricities bunch near $e \sim 0$. Semi-major axes go from $\log[a] \sim 0$ to ~ 2. Orbital periods span near $\log[T_{orbital}] \approx 0$ days. Secondary masses also low ($m_2 \lesssim 1\,M_\odot$). Count grows steadily over 150 Myr.

3.2 Binaries with compact companions

NS-Luminous and BH-Lumionus

Figure 8 shows distributions for the neutron star binaries. Primary mass m_1 concentrates near 1.2–1.6 $M_\odot$, and the count grows from 50 to 150 Myr. Eccentricity distribution peaks near $e \sim 0$, but there is a long tail stretching to $e \sim 0.8$–0.9. Semi-major axes go from $\log[a] \sim 0$ to ~ 2, dominant peak at the low end. Orbital periods are sub-day to about a day short. Secondary mass m_2 spans $\lesssim 1$ to $\sim 6\,M_\odot$. Figure 9 shows BH-luminous star binaries at 50 Myr. Primary mass m_1 sits at 6.5–$8\,M_\odot$. Eccentricities are very low ($e \lesssim 0.05$). Semi-major axis peaks at $\log[a] \sim 2.4$ ($a \sim 250\,R_\odot$), orbital periods around 170–200 days. Tight clustering in a narrow band of parameter space. Secondary mass m_2 is 1.0–1.2 $M_\odot$.

BBH

Figure 10 shows the orbital and mass distributions of BH–BH binaries at 50, 100, and 150 Myr. Both component masses sit in the range $m_1, m_2 \sim 6$–$10\,M_\odot$. This population comes from the most massive stellar progenitors under the Kroupa IMF at solar metallicity. Eccentricity spans nearly the full range $e \sim 0$–1, roughly uniform. Semi-major axes concentrate at large separations—dominant peak at $\log[a] \sim 5$–6 ($a \sim 10^5$–$10^6\,R_\odot$). Orbital periods peak at $\log[T_{orbital}] \sim 8$–10 days. Most BH–BH binaries at these epochs are wide, loosely bound—nowhere near hard enough for efficient gravitational wave inspiral. A secondary population at compact separations ($\log[a] \sim 1$–2) grows from 50 to 150 Myr.

4 DISCUSSION

I have performed 81 simulations of a star cluster with $SFE = 0.17$ and massive primordial binary population combining PeTar with MCLUSTER and AGAMA. They have yielded a substantial number of binary systems with a more or less uniform distribution of mass ratio. Comparing them to parameters of GaiaBH1 and GaiaBH2 and their similarity regions have highlighted certain aspects of sub-population of binaries presented in this work.

Looking at the black hole-luminous companion population of binaries, It must be note that the parameters of these objects are detectable by Gaia telescope. They might not be similar to GaiaBH1 and GaiaBH2, but their companion apparent magnitude suggest that Gaia would have been assess the radial motion of such objects.

One of the important limitation of my work is the uniform distribution of mass ratio. Kotko et al. argue that binary systems in isolated evolution had to have progenitor masses $\sim 39.7\ M_{\odot}\&\sim 1.2\ M_{\odot}$ ($q = 0.03$) for GaiaBH1 and $\sim 22.6\ M_{\odot}\&\sim 1.1\ M_{\odot}$ (q=0.05) for GaiaBH2 to form[16]. Our initial mass ratio distribution spans $q \in [0.1, 1]$, which does not capture parings mentioned in their work. In future simulations, we will need to reconsider paring method for our primordial binaries. Possibly, it will allows us to have GaiaBHs within escaped binary population.

Our clusters have much less dynamically formed binaries compared to primordial population, which is expected as the cluster model is sparse. Our cluster is not able to produce triple or quadruple interactions, though Li et al. argue that GaiaBH1 might be a product of a hierarchical triple system, where inner binary system resulted in a merge leaving a system similar to GaiaBH1 [19]. This scenario could be explored in our simulation either through increase in initial star number or in initial density of a cluster.

5 CONCLUSION

This work ran 81 N-body simulations of young open star clusters undergoing instantaneous gas expulsion, testing whether compact-star binaries with Gaia-like parameters can form dynamically. Using MCLUSTER, AGAMA, and PeTar with full stellar evolution, the simulations produced 4006 binary systems: 271 black hole–luminous star pairs, 484 neutron star–luminous star pairs, and 144 black hole–black hole pairs.

The black hole–luminous companions sat at orbital periods of $170 - 200$ days, with near-circular orbits ($e \lesssim 0.05$) and masses around $1.0 - 1.2\ M_{\odot}$. This narrow region sits right in Gaia's detectability window. If these systems form dynamically in young clusters, Gaia should be able to spot them. The black hole–black hole population, by contrast, was mostly wide pairs at 10^5–$10^6\ R_{\odot}$, too loose to inspiral within a Hubble time.

There are limitations that needed to be addressed. The mass-ratio distribution runs $q \in [0.1, 1.0]$, missing the extreme mass-ratio pairs ($q \sim 0.03 - 0.05$) that isolated binary evolution models say are needed for GaiaBH1 and GaiaBH2. The clusters were also relatively sparse, producing fewer dynamically formed binaries than primordial ones, so exchange interactions which other work shows are crucial for Gaia-like configurations were not well sampled. Future runs will use denser clusters, a range of metallicities, and more particles to narrow down how efficiently dynamical formation produces the wide black hole binaries Gaia can detect.

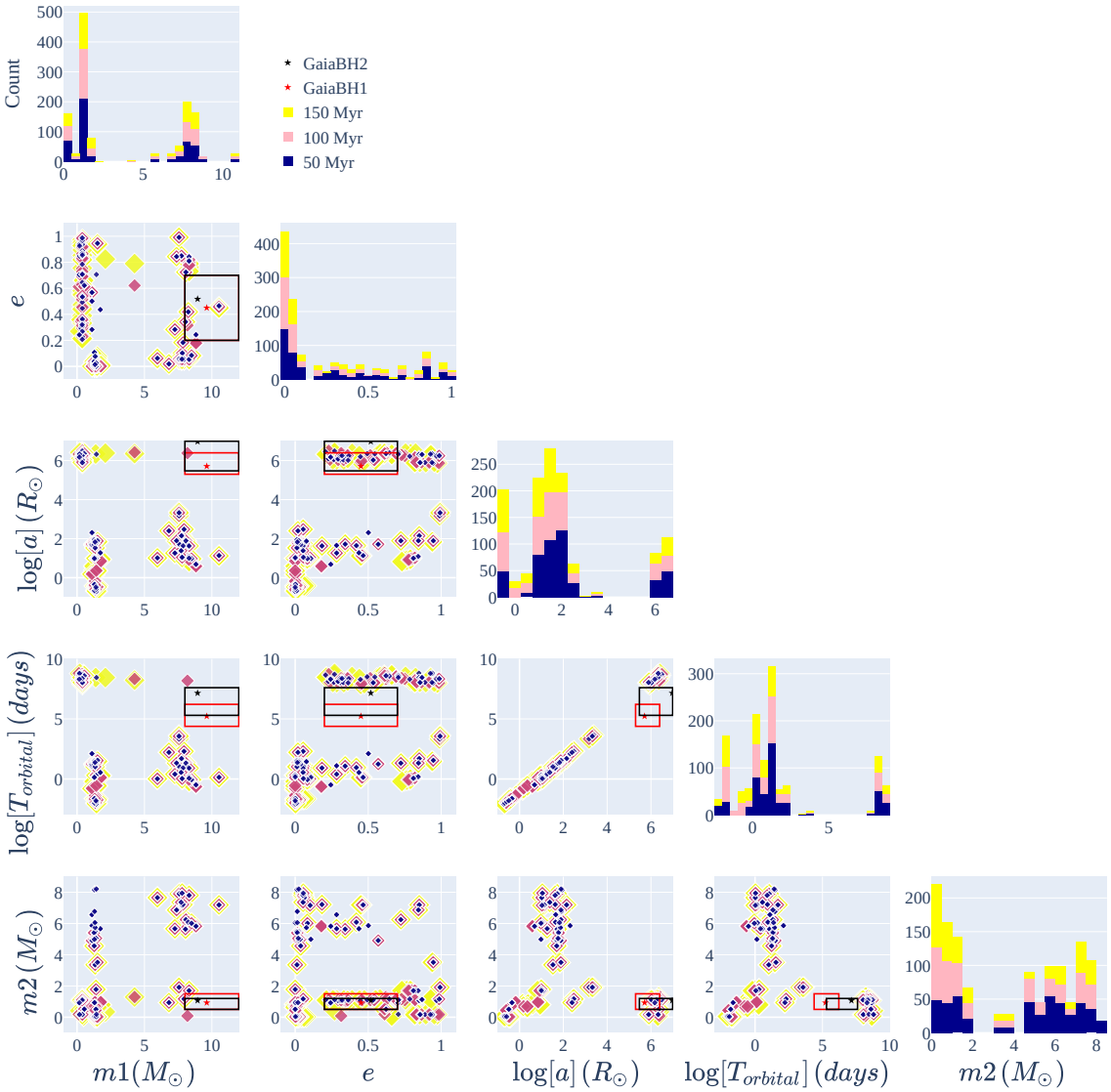

Figure 3: Corner plot of pairwise parameter distributions for binaries from all simulated clusters. The five parameters are initial primary mass (m_1), eccentricity (e), log semi-major axis ($\log[a]$), log orbital period ($\log[T_{orbital}]$), and initial companion mass (m_2). Points are color-coded by snapshot time: 50 Myr (darkblue), 100 Myr (lightpink), 150 Myr (yellow). Red and black stars mark Gaia BH1 and Gaia BH2 parameters. Black and red boxes show the similarity regions used to select Gaia BH1-like and Gaia BH2-like systems, with bounds on m_1, m_2, e, a, and $T_{orbital}$ from Fantoccolli et. el. [14]. Diagonal panels give the 1D marginalized counts for each parameter.

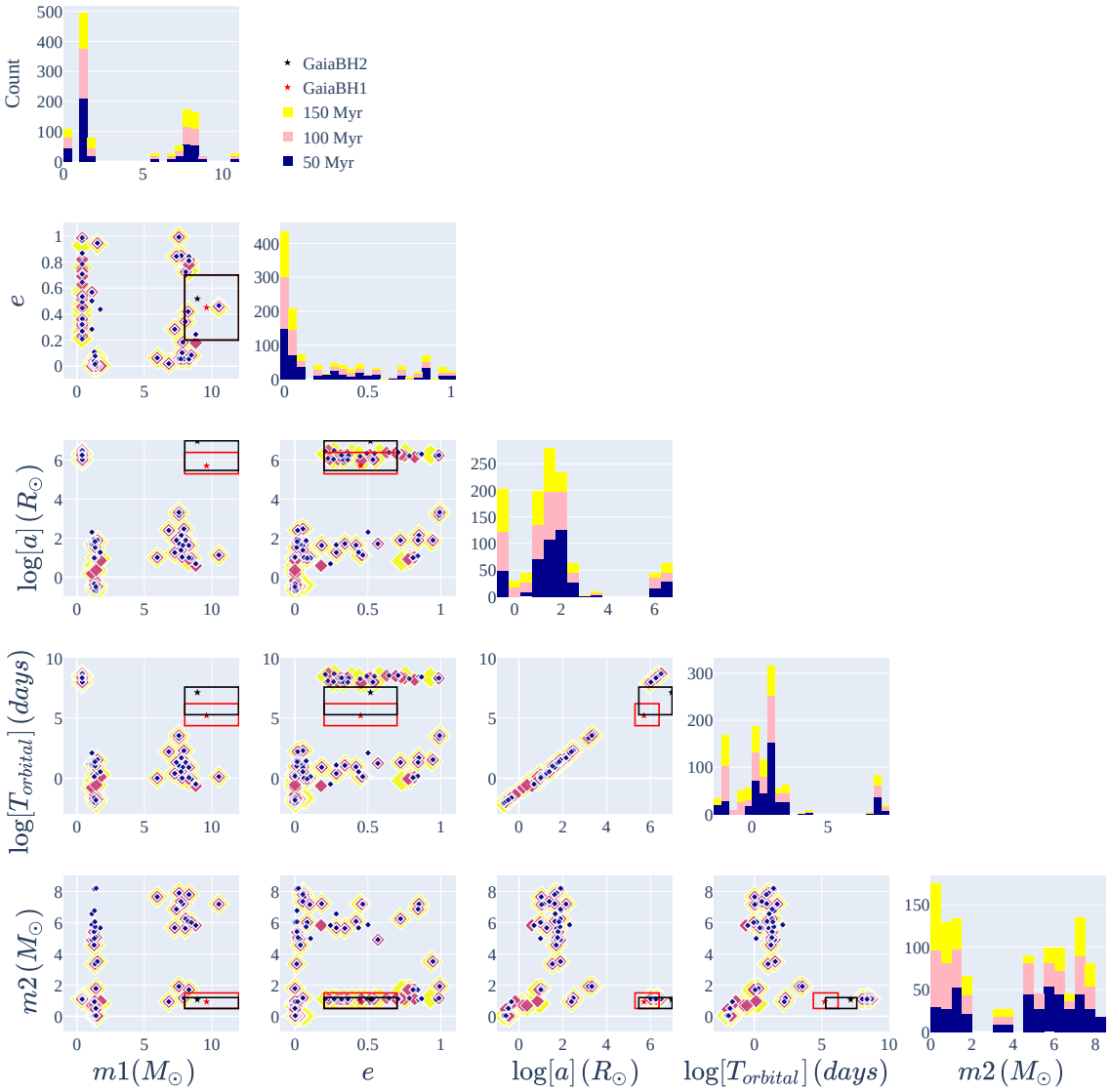

Figure 4: Corner plot of pairwise parameter distributions for primordial binary systems from simulated clusters. The five parameters are initial primary mass (m_1), eccentricity (e), log semi-major axis ($\log[a]$), log orbital period ($\log[T_{orbital}]$), and initial companion mass (m_2). Points are color-coded by snapshot time: 50 Myr (darkblue), 100 Myr (light-pink), 150 Myr (yellow). Red and black stars mark Gaia BH1 and Gaia BH2 parameters. Black and red boxes show the similarity regions used to select Gaia BH1-like and Gaia BH2-like systems, with bounds on m_1, m_2, e, a, and $T_{orbital}$ from Fantoccolli et. el. [14]. Diagonal panels give the 1D marginalized counts for each parameter.

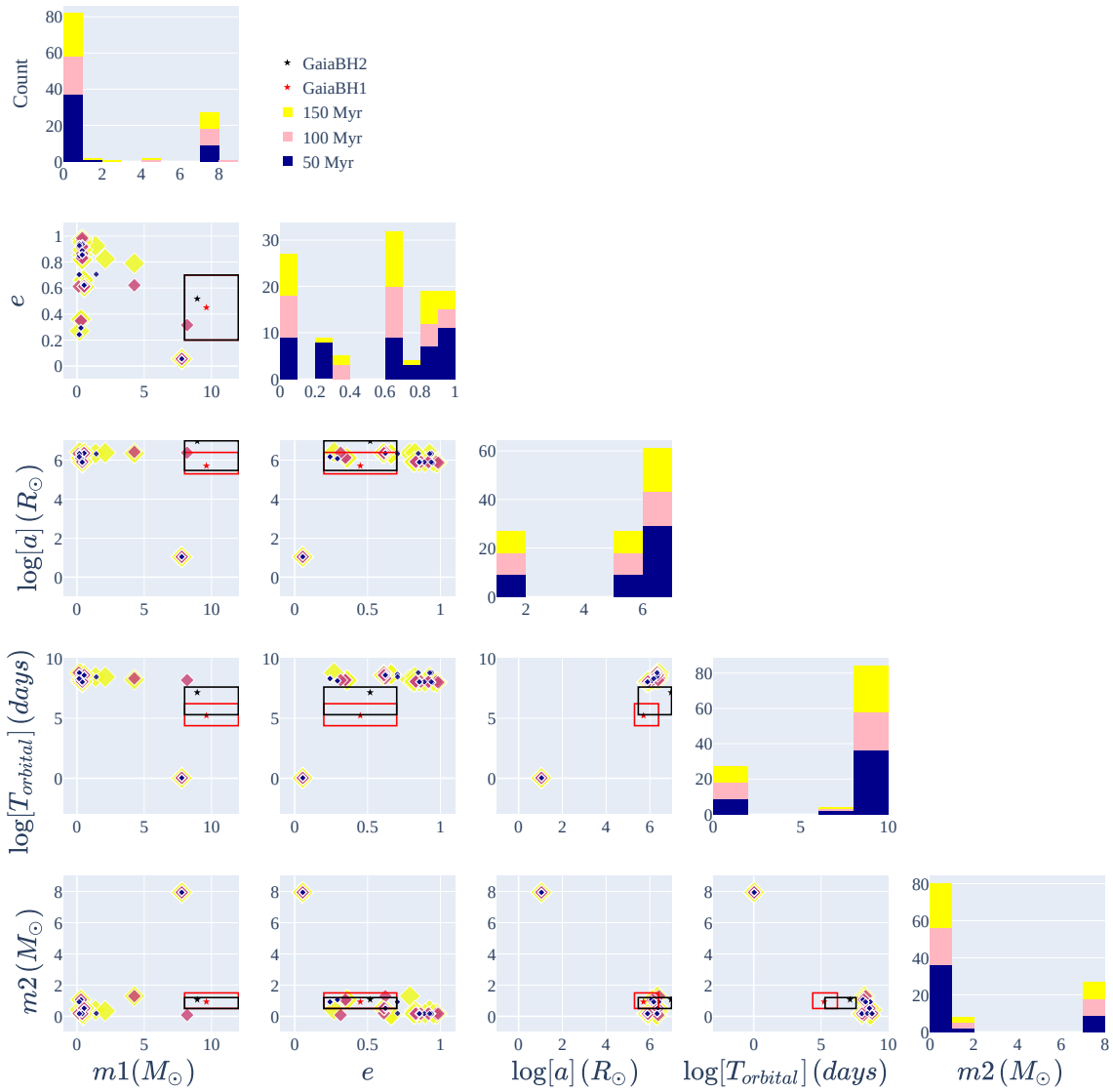

Figure 5: Corner plot of pairwise parameter distributions for dynamical binary systems from simulated clusters. The five parameters are initial primary mass (m_1), eccentricity (e), log semi-major axis ($\log[a]$), log orbital period ($\log[T_{orbital}]$), and initial companion mass (m_2). Points are color-coded by snapshot time: 50 Myr (darkblue), 100 Myr (light-pink), 150 Myr (yellow). Red and black stars mark Gaia BH1 and Gaia BH2 parameters. Black and red boxes show the similarity regions used to select Gaia BH1-like and Gaia BH2-like systems, with bounds on m_1, m_2, e, a, and $T_{orbital}$ from Fantoccolli et. el. [14]. Diagonal panels give the 1D marginalized counts for each parameter.

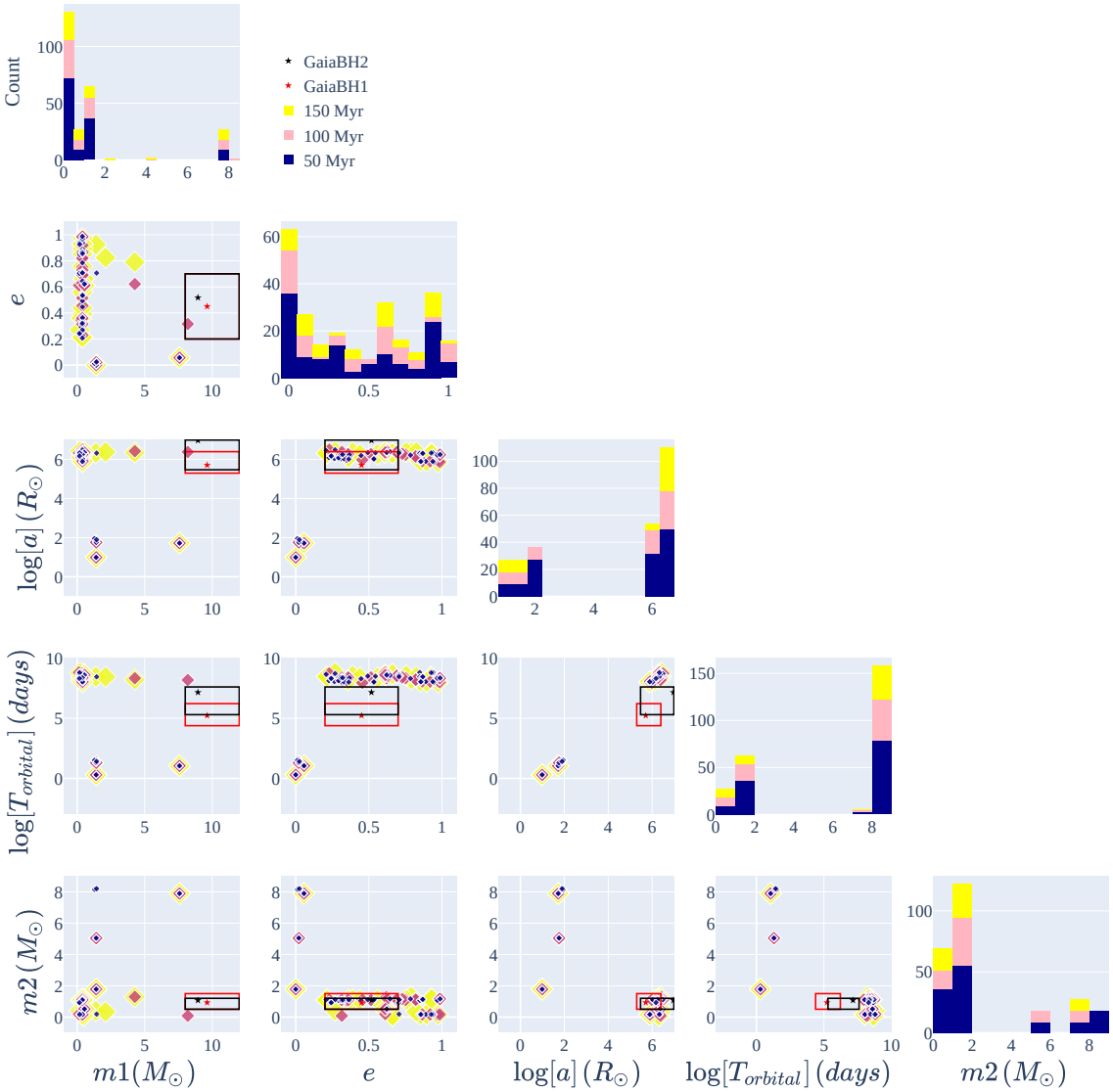

Figure 6: Corner plot of pairwise parameter distributions for retained binaries from all realizations. The five parameters are initial primary mass (m_1), eccentricity (e), log semi-major axis ($\log[a]$), log orbital period ($\log[T_{orbital}]$), and initial companion mass (m_2). Points are color-coded by snapshot time: 50 Myr (darkblue), 100 Myr (lightpink), 150 Myr (yellow). Red and black stars mark Gaia BH1 and Gaia BH2 parameters. Black and red boxes show the similarity regions used to select Gaia BH1-like and Gaia BH2-like systems, with bounds on m_1, m_2, e, a, and $T_{orbital}$ from Fantoccolli et. el. [14]. Diagonal panels give the 1D marginalized counts for each parameter.

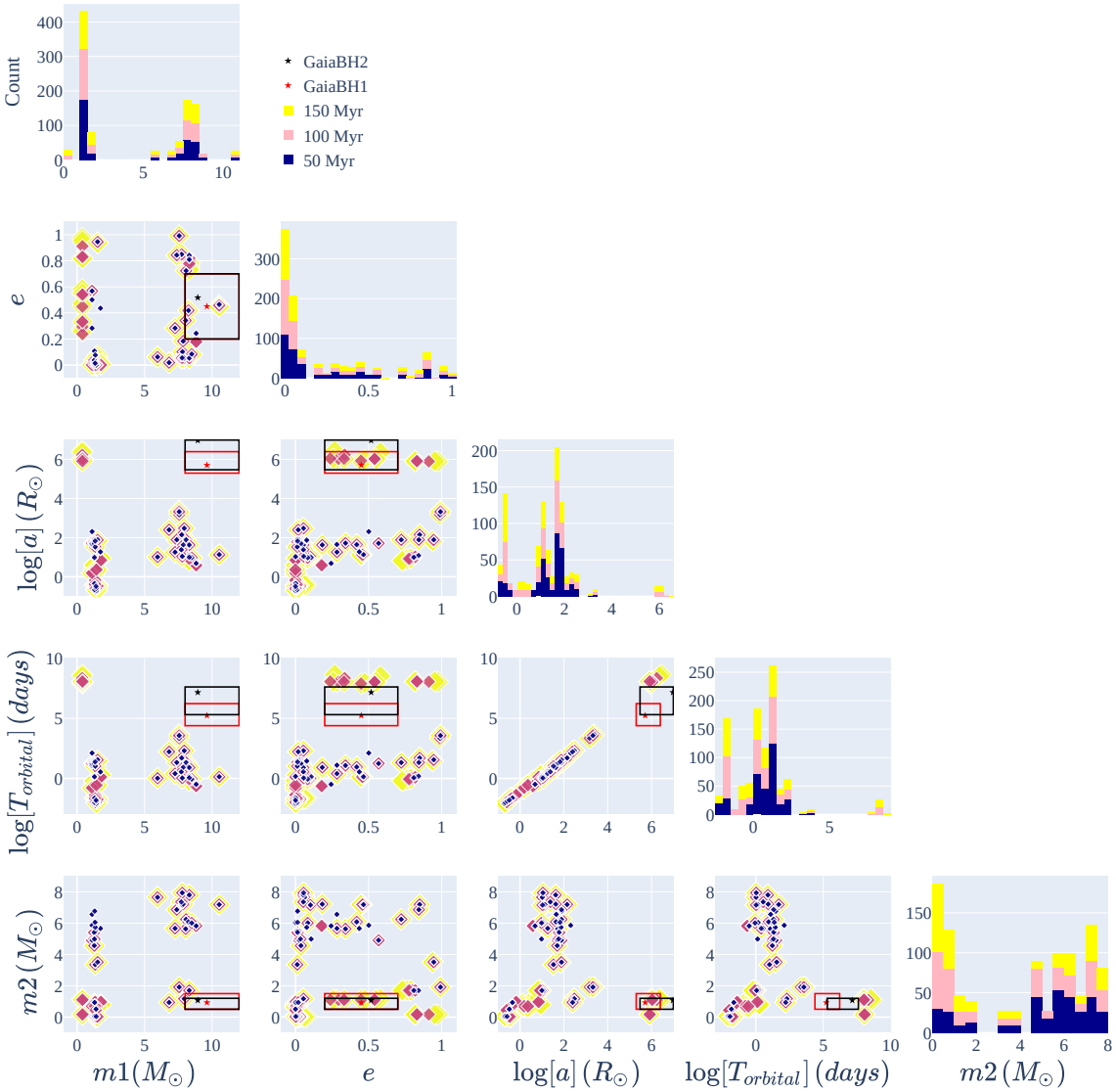

Figure 7: Corner plot of pairwise parameter distributions for escaped binaries from all realizations. The five parameters are initial primary mass (m_1), eccentricity (e), log semi-major axis ($\log[a]$), log orbital period ($\log[T_{orbital}]$), and initial companion mass (m_2). Points are color-coded by snapshot time: 50 Myr (darkblue), 100 Myr (lightpink), 150 Myr (yellow). Red and black stars mark Gaia BH1 and Gaia BH2 parameters. Black and red boxes show the similarity regions used to select Gaia BH1-like and Gaia BH2-like systems, with bounds on m_1, m_2, e, a, and $T_{orbital}$ from Fantoccolli et. el. [14]. Diagonal panels give the 1D marginalized counts for each parameter.

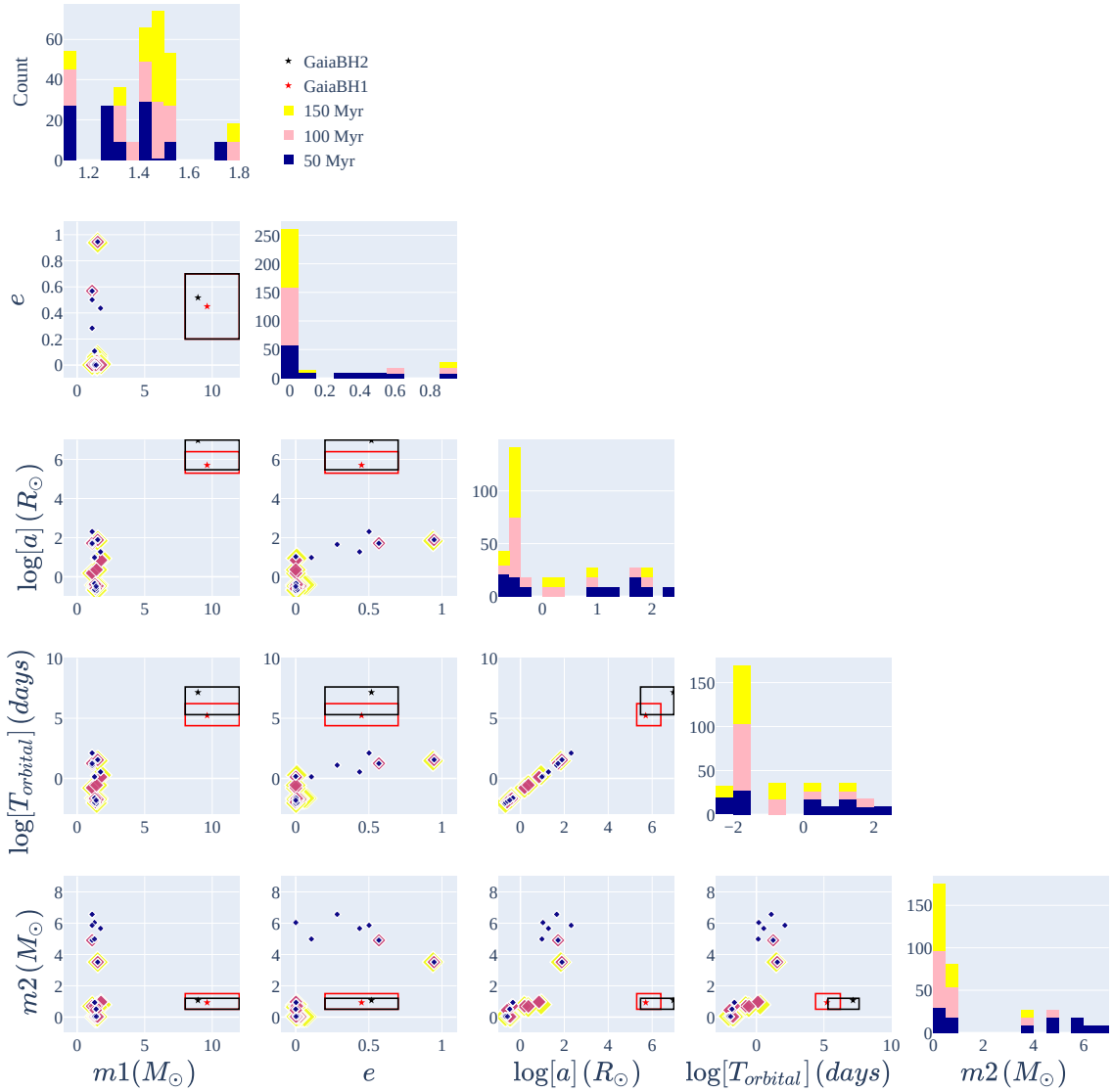

Figure 8: Corner plot of pairwise parameter distributions for neutron star-luminous companion binaries. The five parameters are initial primary mass (m_1), eccentricity (e), log semi-major axis ($\log[a]$), log orbital period ($\log[T_{orbital}]$), and initial companion mass (m_2). Points are color-coded by snapshot time: 50 Myr (darkblue), 100 Myr (lightpink), 150 Myr (yellow). Red and black stars mark Gaia BH1 and Gaia BH2 parameters. Black and red boxes show the similarity regions used to select Gaia BH1-like and Gaia BH2-like systems, with bounds on m_1, m_2, e, a, and $T_{orbital}$ from Fantoccolli et. el. [14]. Diagonal panels give the 1D marginalized counts for each parameter.

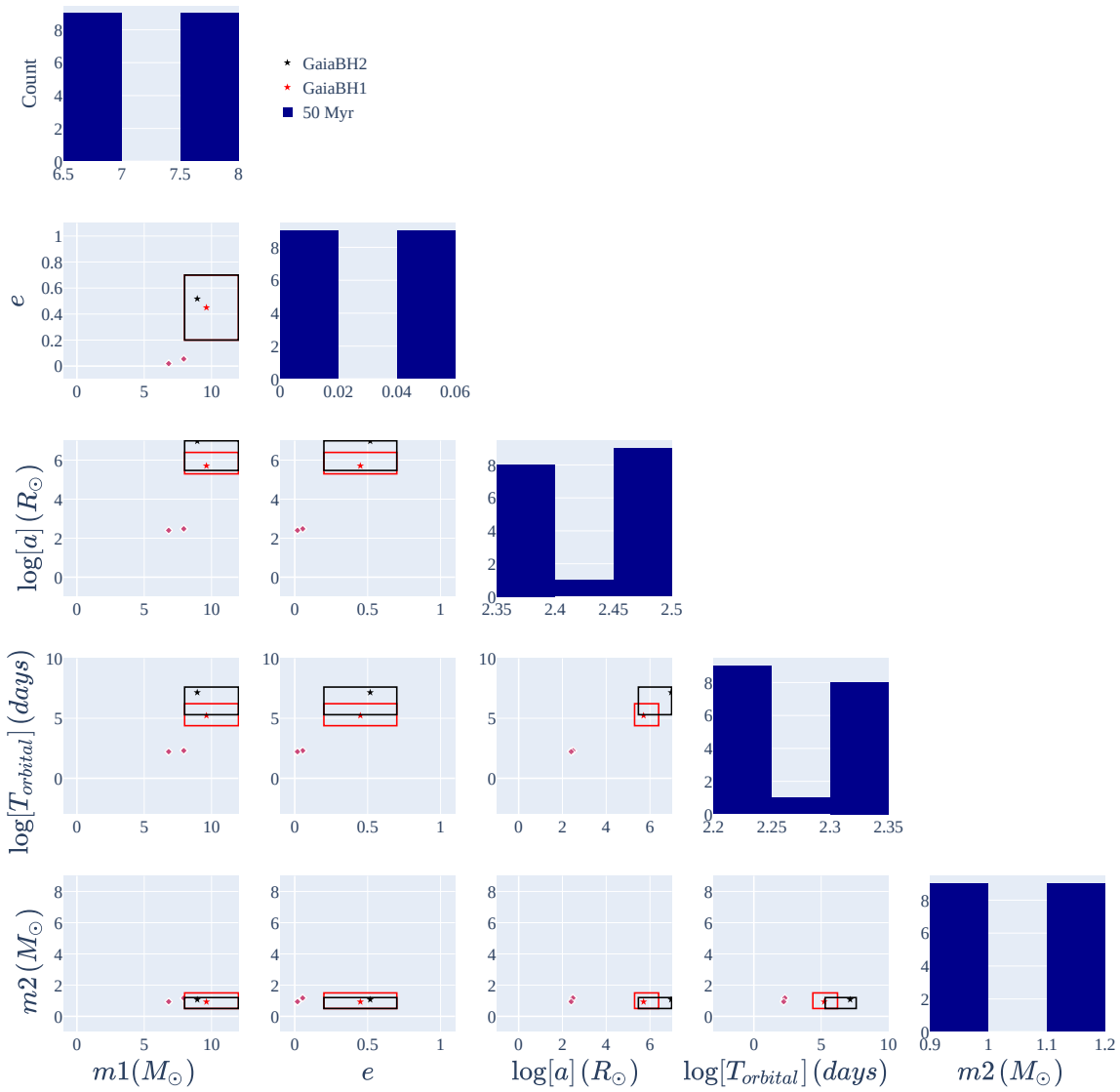

Figure 9: Corner plot of pairwise parameter distributions for black hole-luminous companion binaries. The five parameters are initial primary mass (m_1), eccentricity (e), log semi-major axis ($\log[a]$), log orbital period ($\log[T_{orbital}]$), and initial companion mass (m_2). Points are color-coded by snapshot time: 50 Myr (darkblue), 100 Myr (lightpink), 150 Myr (yellow). Red and black stars mark Gaia BH1 and Gaia BH2 parameters. Black and red boxes show the similarity regions used to select Gaia BH1-like and Gaia BH2-like systems, with bounds on m_1, m_2, e, a, and $T_{orbital}$ from Fantoccolli et. el. [14]. Diagonal panels give the 1D marginalized counts for each parameter.

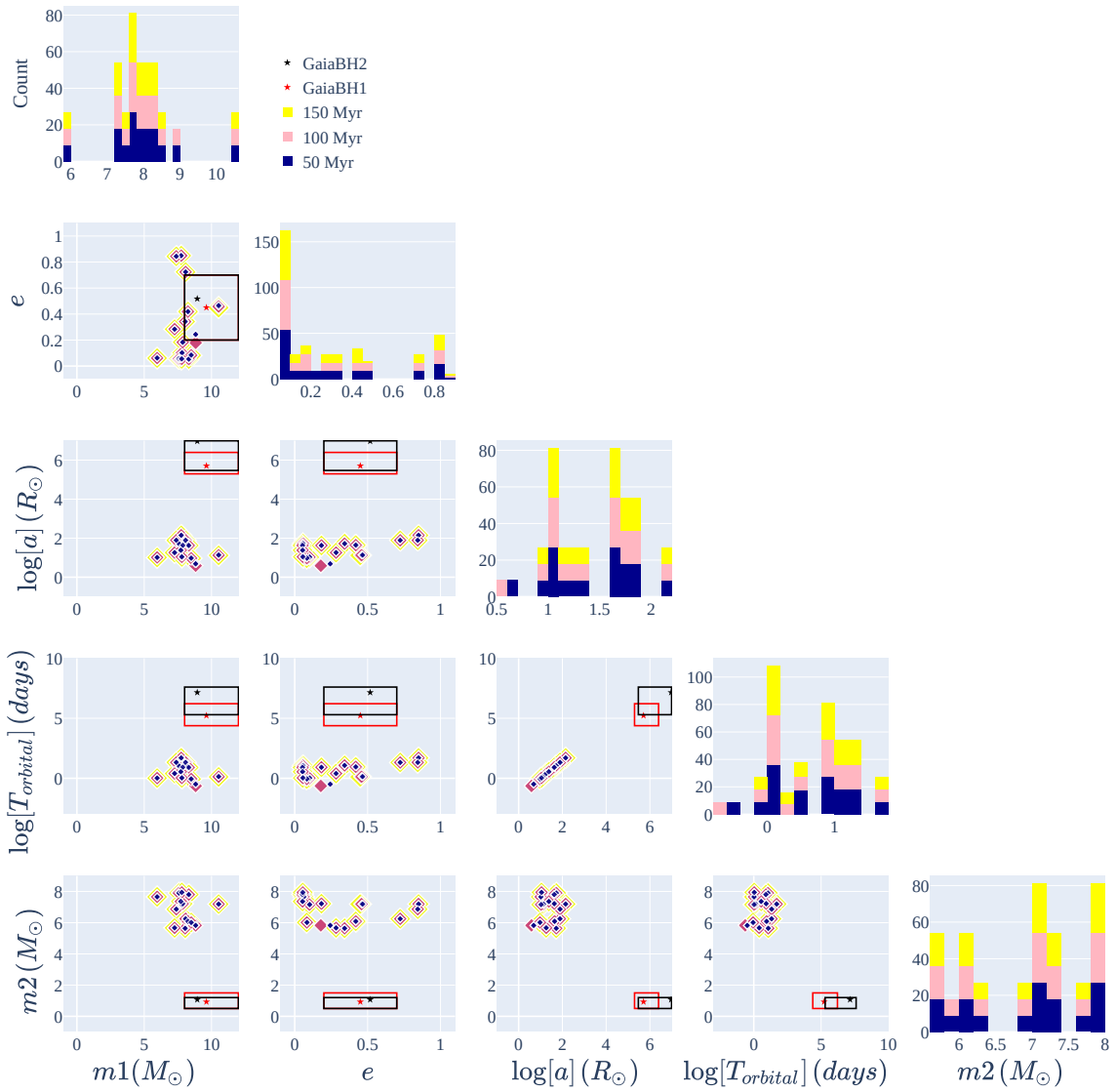

Figure 10: Corner plot of pairwise parameter distributions for binary black holes in our simulations. The five parameters are initial primary mass (m_1), eccentricity (e), log semi-major axis ($\log[a]$), log orbital period ($\log[T_{orbital}]$), and initial companion mass (m_2). Points are color-coded by snapshot time: 50 Myr (darkblue), 100 Myr (lightpink), 150 Myr (yellow). Red and black stars mark Gaia BH1 and Gaia BH2 parameters. Black and red boxes show the similarity regions used to select Gaia BH1-like and Gaia BH2-like systems, with bounds on m_1, m_2, e, a, and $T_{orbital}$ from Fantoccolli et. el. [14]. Diagonal panels give the 1D marginalized counts for each parameter.

REFERENCES

[1] S. Carpano, F. Haberl, and R. Sturm, "Discovery of a 26.2 day period in the long-term X-ray light curve of SXP 1323: a very short orbital period for a long spin period pulsar," **602**, A81 (2017), arXiv:1704.07646 [astro-ph.HE] .

[2] E. Treister and C. M. Urry, "The Cosmic History of Black Hole Growth from Deep Multiwavelength Surveys," Advances in Astronomy **2012**, 516193 (2012), https://onlinelibrary.wiley.com/doi/pdf/10.1155/2012/516193 .

[3] T. M. Heckman and P. N. Best, "The Coevolution of Galaxies and Supermassive Black Holes: Insights from Surveys of the Contemporary Universe," Annual Review of Astronomy and Astrophysics **52**, 589 (2014).

[4] D. G. York, J. Adelman, J. E. Anderson, Jr., S. F. Anderson, J. Annis, N. A. Bahcall, J. A. Bakken, R. Barkhouser, S. Bastian, E. Berman, and et al., "The Sloan Digital Sky Survey: Technical Summary," **120**, 1579 (2000), arXiv:astro-ph/0006396 [astro-ph] .

[5] C. N. Cardamone, C. M. Urry, M. Damen, P. van Dokkum, E. Treister, I. Labbé, S. N. Virani, P. Lira, and E. Gawiser, "Mid-Infrared Properties and Color Selection for X-Ray-Detected Active Galactic Nuclei in the MUSYC Extended Chandra Deep Field-South," **680**, 130 (2008), arXiv:0803.0251 [astro-ph] .

[6] B. Luo, W. N. Brandt, Y. Q. Xue, B. Lehmer, D. M. Alexander, F. E. Bauer, F. Vito, G. Yang, A. R. Basu-Zych, A. Comastri, and et al., "The Chandra Deep Field-South Survey: 7 Ms Source Catalogs," **228**, 2 (2017), arXiv:1611.03501 [astro-ph.GA] .

[7] B. P. Abbott, R. Abbott, T. D. Abbott, M. R. Abernathy, F. Acernese, K. Ackley, C. Adams, T. Adams, P. Addesso, R. X. Adhikari, and et al., "GW150914: The Advanced LIGO Detectors in the Era of First Discoveries," **116**, 131103 (2016), arXiv:1602.03838 [gr-qc] .

[8] B. P. Abbott, R. Abbott, T. D. Abbott, S. Abraham, F. Acernese, K. Ackley, C. Adams, R. X. Adhikari, V. B. Adya, C. Affeldt, and et al., "VizieR Online Data Catalog: Search for GW signals associated with GRBs (Abbott+, 2019)," VizieR On-line Data Catalog: J/ApJ/886/75. Originally published in: 2019ApJ...886...75A (2021).

[9] K. El-Badry, H.-W. Rix, E. Quataert, A. W. Howard, H. Isaacson, J. Fuller, K. Hawkins, K. Breivik, K. W. K. Wong, A. C. Rodriguez, and et al., "A Sun-

like star orbiting a black hole," **518**, 1057 (2023), arXiv:2209.06833 [astro-ph.SR] .

[10] K. El-Badry, H.-W. Rix, Y. Cendes, A. C. Rodriguez, C. Conroy, E. Quataert, K. Hawkins, E. Zari, M. Hobson, K. Breivik, and et al., "A red giant orbiting a black hole," **521**, 4323 (2023), arXiv:2302.07880 [astro-ph.SR] .

[11] Gaia Collaboration, P. Panuzzo, T. Mazeh, F. Arenou, B. Holl, E. Caffau, A. Jorissen, C. Babusiaux, P. Gavras, J. Sahlmann, and et al., "Discovery of a dormant 33 solar-mass black hole in pre-release Gaia astrometry," **686**, L2 (2024), arXiv:2404.10486 [astro-ph.GA] .

[12] P. Nagarajan, K. El-Badry, C. Chawla, U. N. Di Carlo, K. Breivik, C. L. Rodriguez, P. Agrawal, V. Delfavero, and S. Chatterjee, "Realistic Predictions for Gaia Black Hole Discoveries: Comparison of Isolated Binary and Dynamical Formation Models," **137**, 044202 (2025), arXiv:2502.03527 [astro-ph.GA] .

[13] S. Rastello, G. Iorio, M. Mapelli, M. Arca-Sedda, U. N. Di Carlo, G. J. Escobar, T. Shenar, and S. Torniamenti, "Dynamical formation of Gaia BH1 in a young star cluster," **526**, 740 (2023), arXiv:2306.14679 [astro-ph.SR] .

[14] F. Fantoccoli, J. Barber, F. Dosopoulou, D. Chattopadhyay, and F. Antonini, "Properties of black hole-star binaries formed in N-body simulations of massive star clusters: implications for Gaia black holes," **538**, 243 (2025), arXiv:2410.17323 [astro-ph.GA] .

[15] M. Moe and R. Di Stefano, "Mind Your Ps and Qs: The Interrelation between Period (P) and Mass-ratio (Q) Distributions of Binary Stars," **230**, 15 (2017), arXiv:1606.05347 [astro-ph.SR] .

[16] I. Kotko, S. Banerjee, and K. Belczynski, "The enigmatic origin of two dormant BH binaries: Gaia BH1 and Gaia BH2," **535**, 3577 (2024), arXiv:2403.13579 [astro-ph.SR] .

[17] H. P. Preece, A. Vigna-Gómez, A. S. Rajamuthukumar, P. Vynatheya, and J. Klencki, "The Evolution of Massive Stellar Multiplicity in the Field I. Numerical simulations, long-term evolution and final outcomes," arXiv e-prints , arXiv:2412.14022 (2024), arXiv:2412.14022 [astro-ph.SR] .

[18] A. Generozov and H. B. Perets, "A Triple Scenario for the Formation of Wide Black Hole Binaries Such as Gaia BH1," The Astrophysical Journal **964**, 83 (2024).

[19] Z. Li, C. Zhu, X. Lu, G. Lü, L. Li, H. Liu, S. Guo, and J. Yu, "A Possible Formation Scenario of the Gaia BH1: Inner Binary Merger in Triple Systems," **975**, L8 (2024), arXiv:2410.10581 [astro-ph.SR] .

[20] A. Generozov and H. B. Perets, "A Triple Scenario for the Formation of Wide Black Hole Binaries Such as Gaia BH1," **964**, 83 (2024), arXiv:2312.03066 [astro-ph.SR] .

[21] U. N. Di Carlo, P. Agrawal, C. L. Rodriguez, and K. Breivik, "Young Star Clusters Dominate the Production of Detached Black HoleStar Binaries," **965**, 22 (2024), arXiv:2306.13121 [astro-ph.GA] .

[22] A. Tanikawa, L. Wang, and M. S. Fujii, "Compact Binary Formation in Open Star Clusters II: Difficulty of Gaia NS formation in low-mass star clusters," The Open Journal of Astrophysics **7**, 39 (2024), arXiv:2404.01731 [astro-ph.SR] .

[23] A. Leveque, "mcluster," `https://github.com/agostinolev/mcluster.git` (2023).

[24] E. Vasiliev, "AGAMA: action-based galaxy modelling architecture," **482**, 1525 (2019), arXiv:1802.08239 [astro-ph.GA] .

[25] P. Kroupa, "On the variation of the initial mass function," **322**, 231 (2001), arXiv:astro-ph/0009005 [astro-ph] .

[26] D. C. Kiminki and H. A. Kobulnicky, "An Updated Look at Binary Characteristics of Massive Stars in the Cygnus OB2 Association," **751**, 4 (2012), arXiv:1203.2156 [astro-ph.SR] .

[27] H. Sana, S. E. de Mink, A. de Koter, N. Langer, C. J. Evans, M. Gieles, E. Gosset, R. G. Izzard, J.-B. Le Bouquin, and F. R. N. Schneider, "Binary Interaction Dominates the Evolution of Massive Stars," Science **337**, 444 (2012), arXiv:1207.6397 [astro-ph.SR] .

[28] H. A. Kobulnicky, D. C. Kiminki, M. J. Lundquist, J. Burke, J. Chapman, E. Keller, K. Lester, E. K. Rolen, E. Topel, A. Bhattacharjee, and et al., "Toward Complete Statistics of Massive Binary Stars: Penultimate Results from the Cygnus OB2 Radial Velocity Survey," **213**, 34 (2014), arXiv:1406.6655 [astro-ph.SR] .

[29] B. Shukirgaliyev, G. Parmentier, P. Berczik, and A. Just, "Impact of a star formation efficiency profile on the evolution of open clusters," **605**, A119 (2017), arXiv:1706.03228 [astro-ph.GA] .

[30] H. C. Plummer, "On the problem of distribution in globular star clusters," **71**, 460 (1911).

[31] B. Shukirgaliyev, *The Life of Star Clusters, From Birth to Dissolution: A New Approach*, Ph.D. thesis, Astronomisches Rechen-Institut (2018).

[32] J. Bovy, "galpy: A python LIBRARY FOR GALACTIC DYNAMICS," The Astrophysical Journal Supplement Series **216**, 29 (2015).

[33] J. Bovy and H.-W. Rix, "A Direct Dynamical Measurement of the Milky Way's Disk Surface Density Profile, Disk Scale Length, and Dark Matter Profile at 4 kpc ¡~R ¡~9 kpc," **779**, 115 (2013), arXiv:1309.0809 [astro-ph.GA] .

[34] L. Wang, M. Iwasawa, K. Nitadori, and J. Makino, "PETAR: a high-performance N-body code for modelling massive collisional stellar systems," **497**, 536 (2020), arXiv:2006.16560 [astro-ph.IM] .

[35] S. Banerjee, K. Belczynski, C. L. Fryer, P. Berczik, J. R. Hurley, R. Spurzem, and L. Wang, "BSE versus StarTrack: Implementations of new wind, remnant-formation, and natal-kick schemes in NBODY7 and their astrophysical consequences," **639**, A41 (2020), arXiv:1902.07718 [astro-ph.SR] .

[36] K. Belczynski, T. Bulik, C. L. Fryer, A. Ruiter, F. Valsecchi, J. S. Vink, and J. R. Hurley, "On the Maximum Mass of Stellar Black Holes," **714**, 1217 (2010), arXiv:0904.2784 [astro-ph.SR] .

[37] J. R. Hurley, O. R. Pols, and C. A. Tout, "Comprehensive analytic formulae for stellar evolution as a function of mass and metallicity," **315**, 543 (2000), arXiv:astro-ph/0001295 [astro-ph] .

[38] C. L. Fryer, K. Belczynski, G. Wiktorowicz, M. Dominik, V. Kalogera, and D. E. Holz, "Compact Remnant Mass Function: Dependence on the Explosion Mechanism and Metallicity," **749**, 91 (2012), arXiv:1110.1726 [astro-ph.SR] .

[39] K. Belczynski, A. Heger, W. Gladysz, A. J. Ruiter, S. Woosley, G. Wiktorowicz, H.-Y. Chen, T. Bulik, R. O'Shaughnessy, D. E. Holz, and et al., "The effect of pair-instability mass loss on black-hole mergers," **594**, A97 (2016), arXiv:1607.03116 [astro-ph.HE] .